Efficient simulation of chromatographic separation processes

Solomon F. Brown[a,*], Mark D. Ogden[a], Eric S. Fraga[b]

[a]*Department of Chemical and Biological Engineering, The University of Sheffield, Sheffield*
[b]*Centre for Process Systems Engineering (CPSE), Department of Chemical Engineering, UCL (University College London), London*

Abstract

This work presents the development and testing of an efficient, high resolution algorithm developed for the solution of equilibrium and non-equilibrium chromatographic problems as a means of simultaneously producing high fidelity predictions with a minimal increase in computational cost. The method involves the coupling of a high-order WENO scheme, adapted for use on non-uniform grids, with a piecewise adaptive grid (PAG) method to reduce runtime while accurately resolving the sharp gradients observed in the processes under investigation. Application of the method to a series of benchmark chromatographic test cases, within which an increasing number of components are included over short and long spatial domains and containing shocks, shows that the method is able to accurately resolve the discontinuities and that the use of the PAG method results in a reduction in the CPU runtime of upto 90 %, without degradation of the solution, relative to an equivalent uniform grid.

Keywords: Column Chromatography, WENO scheme, Adaptive Mesh Refinement

Introduction

Chromatography is an effective process which plays a central role in a great many industrial separation and purification systems. Not surprisingly therefore, the modelling and optimisation of these processes has received a great deal of attention in recent years (von Lieres and Andersson, 2010; Enmark et al., 2011; Close et al., 2014; Zhang et al., 2017; Hahn et al., 2014). A particular case is liquid batch chromatography, which is achieved by the injection of a pulse of solute into the chromatographic column where the differential adsorption results in the separation of the solute between the liquid and solid phases. The steep fronts that occur during such an operation can be a particular challenge to simulate due to the discontinuities that may form in the solution profile (Mazzotti, 2009).

A number of models of increasing complexity have been proposed for modelling chromatography problems (Guiochon et al., 2006), notably the general rate model (GRM) (Guiochon et al., 2006; Püttmann et al., 2016), lumped kinetic model (LKM) (Zhang et al., 2017; Pais et al., 1998) and equilibrium-dispersion model (EDM) (Enmark et al., 2011; Chan et al., 2008). All of these models effectively describe the convection dominated flow of the solute through the bed along with mass transfer with the stationary phase. These models are composed of complex systems of partial

*Corresponding author
Email address: s.f.brown@sheffield.ac.uk (Solomon F. Brown)

differential-algebraic equations (PDAE), for which a particular challenge is numerically resolving the formation of discontinuities, or shock waves, in the solution profiles.

A number of high resolution numerical schemes with the ability to resolve these shocks have been proposed and applied in the literature, ranging from Finite Volume flux-limiting based (Javeed et al., 2011b; Medi and Amanullah, 2011), weighted essentially non-oscillatory (WENO) (von Lieres and Andersson, 2010) to Discontinuous Galerkin Finite Element (Javeed et al., 2011a) methods. However, an important aspect to consider when selecting an appropriate numerical method is that the simulation of a single process is often performed as part of either an estimation of parameters (Hahn et al., 2014; Püttmann et al., 2016) against experimental data or for the optimisation of a process design, and hence the solution of a large number of simulations is required. Computational efficiency of the scheme selected is therefore key. While they deliver greater accuracy, one disadvantage of the use of high resolution schemes described above is that they necessarily result in an increase in the CPU run times over simpler, though less accurate, methods. As additional computational weight is proportional to the size of the discretisation, one means of addressing this issue is to adopt an adaptive mesh refinement (AMR) strategy to reduce the mesh size used.

The application of AMR for CFD is widespread (Pelanti and LeVeque, 2006; Gourma et al., 2013; Brown et al., 2014), with various methodologies applied ranging from the popular hierarchical box-structured techniques, first described by Berger and Oliger (1984), to moving grid methods (see for example Tang and Tang, 2003; Kelling et al., 2014; Coimbra et al., 2004; Sereno et al., 1991). While not requiring such complex data structures as the former, the moving grid technique has the drawback of requiring the solution of additional equations. The Piecewise Uniform Adaptive Grid (PAG) method (Fraga and Morris, 1996; Brown et al., 2015a), originally developed for the capture of soliton waves in dispersive wave equations, benefits from a relatively simple structure. It employs a single, piecewise uniform grid in which the spatial discretisation and time stepping algorithm are wholly decoupled and the opportunity to apply various solvers for the temporal evolution of the problem exists.

The use of the PAG method requires the use of numerical schemes which may be applied to non-uniform meshes. Most Finite Volume schemes, however, assume uniformity in the discretisation. Additionally, while the Discontinuous Galerkin method is inherently geometrically flexible to deal with discontinuities, it is necessary either to apply a limiter (Javeed et al., 2011a), which has been shown to introduce errors in the steady state profile, or to include artificial diffusion. Recently however, a high order compact, central WENO reconstruction has been developed for non-uniform grids which provides the geometric flexibility required for use with PAG (Semplice et al., 2015).

A disadvantage of using high resolution schemes, such as WENO, in problems containing steep gradients is that there is commonly a necessity to include additional artificial diffusion to ensure the convergence of the implicit Backwards Difference Formula (BDF) methods (see, for example, von Lieres and Andersson, 2010) typically applied for temporal resolution. Given that the explicit modelling of mass transfer in the GRM and LKM can result in stiff behaviour, an implicit temporal solver is required; however, the use of Implicit-Explicit (IMEX) Runge Kutta methods (Ascher et al., 1997), where the potentially stiff mass transfer and the convection-diffusion terms are treated essentially independently using implicit and explicit techniques respectively, offer the ability to resolve both the mass transfer

dynamics and sharp gradients without resorting to artificial diffusion.

The purpose of this work is two-fold, firstly we present the application of the compact WENO reconstruction to an upwind scheme for chromatography problems and investigate the effectiveness of the PAG method in reducing the computational runtime associated with the use of this third order scheme. Secondly, the efficacy of the IMEX, relative to BDF, methods in solving relevant problems, in terms of accuracy and computational efficiency, is investigated.

This work is arranged as follows. Section 2 presents the non-equilibrium and equilibrium chromatography models used and Section 3 presents briefly the PAG adaptive grid algorithm. Section 4 describes the numerical methods, Section 4.1 presents the spatial discretisation including the compact upwind WENO scheme applied herein, and Section 4.2 presents the implicit and implicit-explicit temporal solvers that are tested. Four numerical case studies are used to demonstrate the effectiveness and efficiency of the combined adaptive grid and numerical schemes considered.

The Lumped Kinetic Model (LKM)

In this work, the non-equilibrium LKM for chromatography is used. This accounts for the internal and external mass transport resistances with a mass transfer coefficient, k. The model assumes that the bed is isothermal and packed homogeneously, while the radial gradients are neglected. With these assumptions the mass balance equations for species n can be written as:

$$\frac{\partial c_n}{\partial t} + v\frac{\partial c_n}{\partial x} = D_a\frac{\partial^2 c_n}{\partial x^2} + k_a\frac{q_n - q_n^*}{\epsilon} \tag{1}$$

$$\frac{\partial q_n}{\partial t} = -k_a\frac{q_n - q_n^*}{(1-\epsilon)} \tag{2}$$

$$q_n^* = f\left(c_n\right) \tag{3}$$

for $n = 1, 2, \ldots, N_c$ and where N_c is the number of species in the mixture, c_n and q_n are the liquid concentration and solid concentration of component n respectively, v is the interstitial velocity, ϵ is the porosity, D_a is the dispersion coefficient while t and x are the time and axial coordinates respectively. q_n^* is equilibrium relationship for the nth component which describes thermodynamics behaviour underlying the chromatographic separation process and f is the associated isotherm.

An alternative model, the Equilibrium Dispersive Model (EDM) which is a limiting case of the LKM, is also considered in the study as it retains the spatial behaviour of the LKM without the additional relaxation behaviour that requires the application of a complex temporal solver; furthermore, this simpler model admits analytical solutions in simple cases. The EDM results from taking the limit $k_n \to \infty$, so that mass transfer is assumed to occur instantaneously. The resulting set of equations is:

$$\frac{\partial c_n}{\partial t} + \frac{1-\epsilon}{\epsilon}\frac{\partial q_n}{\partial t} + v\frac{\partial c_n}{\partial x} = D_a\frac{\partial^2 c_n}{\partial x^2} \quad (4)$$

$$q_n = f(c_n),\ n = 1, 2, \ldots, N_c \quad (5)$$

In order to close the above model, appropriate initial and boundary conditions must be imposed for each problem. Where not described explicitly in Section 5 it is assumed that the domain is initially empty (i.e. $c_n = 0, n = 1, 2, \ldots, N_c$); similarly, unless otherwise stated the problems involve the injection of a species concentration into the domain from the left hand boundary and a Neumann condition is imposed on the right.

The piecewise uniform adaptive grid (PAG) method

The PAG method (Fraga and Morris, 1992, 1996; Brown et al., 2015a) is based on identifying regions of the spatial domain that require refinement through the analysis of the geometry of the solution profile. The original application domain was the solution of *soliton*-generating (Zabusky and Kruskal, 1965) nonlinear dispersive wave equations. Geometric analysis was used to identify the locations of solitons, based on the assumption that the critical regions of the spatial domain were those where the solitons were present. No other criteria, such as *a posteriori* error estimation, were used in defining the adapted grid. Subsequently, the method was applied to the simulation of a fixed bed reactor system (Fraga, 1998) where the geometric analysis was applied to a numerical approximation of the first derivative of the solution profile. This enabled the method to refine the grid in locations of high gradients.

An important property of the grid generated by this method is that the points are distributed in a *piecewise-uniform* fashion. This was motivated by the observation that many numerical methods, both for discretisation in the spatial dimension and for time-stepping, have been developed with an implicit assumption of uniformity in the grid spacing. When non-uniformity is present, these methods often suffer losses in accuracy, typically losing one order of accuracy, and become more susceptible to stability issues (Russell and Christiansen, 1978). It was found that if non-uniformity in the adapted grid were present in regions that were not critical, i.e. those where a coarser grid was appropriate, problems with accuracy and stability were minimised. Hence, the PAG method was constructed to generate a nonuniform grid which consists of a set of contiguous non-overlapping uniform sub-meshes, without requiring the use of artificial internal boundary conditions as is necessary for hierarchical box-structured AMR methods.

The basic approach of the PAG method can be summarised as follows: locate each soliton in the solution, place a fine mesh, with uniform spacing h_{goal}, so as to cover the support for each soliton and fill in the gaps between each fine mesh with more coarsely spaced points. For application to problems with sharp gradients, the method is applied using the profile of the absolute value of the numerical approximation to the gradient instead of the solution profile itself. Each sub-interval identified, be it the support for a soliton (or a region with a sharp gradient) or the gap between two such support regions, is discretised uniformly. The support regions are discretised finely; the other sub-intervals used coarser discretisations, with increasing coarseness away from the support regions. However, any numerical method

used will work on the whole mesh at once, considering it to be a nonuniform mesh overall.

Once the new mesh has been developed, a question arises as to the means of transferring the solution from the old grid to the new one. Fraga and Morris (1996) suggested the use of quadratic or cubic interpolation over a simpler linear interpolation; they showed that the latter would increase the dissipation of the solution. However, only the linear interpolation has practically been found to be effective in the case of shocks (Fraga, 1998; Brown et al., 2014) due to oscillations introduced during the reconstruction phase when using higher order interpolations. Given that, in the current work, a non-oscillatory reconstruction is used during the solution process, the use of the same polynomial when transferring the solution from one mesh to another may provide a means for reducing the dissipation introduced during this step. A comparison of the predictions obtained using the linear (PAG-linear) and WENO (PAG-WENO) based reconstructions will be included in the analysis presented in Section 5.

Numerical Method

To apply a numerical method to the system of equations (1-3), the governing equations are first written in the general form:

$$\frac{\partial u}{\partial t} + \frac{\partial F(u)}{\partial x} = D\frac{\partial^2 u}{\partial x^2} + \frac{(u - u^*)}{\epsilon\,(u)} \tag{6}$$

The numerical solution of the above equation utilises the Method of Lines (MoL), which requires appropriate temporal and spatial discretisations; a description of these follow.

Spatial discretisation

As described above, it is necessary to account for the non-uniformity explicitly in the selection of suitable spatial schemes to accommodate the non-uniform size of the computational cells that form the mesh when the PAG is applied. An appropriate scheme, based on a WENO reconstruction using a compact nonuniform stencil, was originally suggested by Levy et al. (2000) and was recently investigated by Semplice et al. (2015) in the context of central methods (Semplice et al., 2015); however in this work, this WENO reconstruction is utilised in an upwind method. To this end we first of assume that $u\,(x)$ is defined in $\Omega = [a, b]$, of which $\{\Omega_j : j = 1, \ldots, N\}$ is a partition and we take U_j to be average of u on Ω_j, i.e.:

$$U_j = \frac{1}{h_j}\int_{\Omega_j} u\,(x)\,dx, \qquad j = 1, \ldots, N. \tag{7}$$

then integrating equation (6) over a cell, Ω_j, with $h_j = |\Omega_j|$ gives:

$$\frac{\partial U_j}{\partial t} = -\frac{1}{h_j}\left(F(u_{j+\frac{1}{2}}) - F(u_{j-\frac{1}{2}})\right) + D\frac{1}{h_j}\left(\left(\frac{\partial u}{\partial x}\right)_{j+\frac{1}{2}} - \left(\frac{\partial u}{\partial x}\right)_{j-\frac{1}{2}}\right) + \frac{1}{h_j}\int_{\Omega_j}\frac{(u - u^*)}{\epsilon\,(u)}dx \tag{8}$$

Again, for Ω_j, we take the third order polynomial which satisfies conservation in the cell and its two neighbours Ω_{j+i}, where $i = -1, 1$; this polynomial is described as the *optimal* polynomial $P_{opt}(x)$:

$$\frac{1}{h_{j+i}} \int_{\Omega_{j+i}} P_{opt}(x)dx = U_{j+i}, \qquad i = -1, 0, 1 \tag{9}$$

This polynomial is completely determined by these conditions, and is given by:

$$P_{opt}(x) = U_j + p_x(x - x_j) + \frac{1}{2}p_{xx}\left((x - x_j)^2 - \frac{h_j}{12}\right), \tag{10}$$

where

$$p_x = \frac{(h_j + 2h_{j-1})\, U[j-1; j] + (h_j + 2h_{j+1})\, U[j; j+1]}{2\,(h_{j-1} + h_j + h_{j+1})} \tag{11}$$

and

$$p_{xx} = \frac{3\,(2h_j + h_{j-1} + h_j + 1)\, U[j-1; j; j+1]}{2\,(h_{j-1} + h_j + h_{j+1})} \tag{12}$$

where the divided difference formulae are

$$U[j-1; j] = \frac{U_j - U_{j-1}}{x_j - x_{j-1}} \tag{13}$$

$$U[j-1; j; j+1] = \frac{U[j-1; j] - U[j; j+1]}{x_{j+1} - x_{j-1}} \tag{14}$$

In order to define a non-oscillatory polynomial in the case of a non-smooth u we define:

$$P_\gamma(x) = U_j + U[j - 2 + \gamma; j - 1 + \gamma]\,(x - x_j),\ \gamma = 1, 2 \tag{15}$$

along with

$$P_{opt} = \alpha_0 P_0 + \sum_{\gamma=1}^{2} \alpha_\gamma P_\gamma, \tag{16}$$

and $\alpha_0 = 1/2$ and $\alpha_\gamma = 1/4$ for $\gamma = 1, 2$. Finally, these coefficients are weighted using smoothness functions (β) so that the final polynomial reconstruction is:

$$P = \tilde{\alpha}_0 P_0 + \sum_{\gamma=1}^{2} \tilde{\alpha}_\gamma P_\gamma \tag{17}$$

where

$$\tilde{\alpha} = \frac{\omega_\gamma}{\sum_{\delta=0}^{2} \omega_\delta}, \omega_\gamma = \frac{\alpha_\gamma}{(\epsilon + \beta_\gamma)^2},\ \gamma = 0, 1, 2. \tag{18}$$

and the smoothness functions are given by:

$$\beta_0 = \frac{13}{12} h_j^4 p_{xx}^2 + h_j^2 p_x^2 \tag{19}$$

$$\beta_1 = U[j-1; j]^2 h_j^2 \tag{20}$$

$$\beta_2 = U[j; j+1]^2 h_j^2. \tag{21}$$

Temporal discretisation

Relaxation equations of the form (6) may contain disparate time scales representing various interacting processes. This results in a stiffness of the equations (Butcher, 2008) which typically means that implicit methods, such as the Backwards Difference Formulae (BDF) methods (for example as implemented in IDA Hindmarsh et al., 2005), are used to solve them. The disadvantage of this is that the spatial resolution of the movement of sharp fronts can prove difficult and requires the addition of additional numerical diffusion (von Lieres and Andersson, 2010). Instead, a fourth order IMEX Runge-Kutta is applied here. IMEX methods consist of applying, sequentially, an implicit and explicit discretisation; this allows the separate solution of stiff and non-stiff parts of the equations without the introduction of numerical diffusion in the spatial discretisation or a prohibitively small time step to account for the relaxation phenomena within an explicit method.

When applied to the system 6, they take the form:

$$u^{(i)} = u^n - \delta t \sum_{j=1}^{i-1} \tilde{a}_{ij} \left(\frac{\partial F(u^{(j)})}{\partial x} - D \frac{\partial^2 u^{(j)}}{\partial x^2} \right) + \delta t \sum_{j=1}^{\nu} a_{ij} R(u^{(j)}) \tag{22}$$

$$u^{n+1} = u^n - \delta t \sum_{i=1}^{\nu} \tilde{w}_i \left(\frac{\partial F(u^{(i)})}{\partial x} - D \frac{\partial^2 u^{(i)}}{\partial x^2} \right) + \delta t \sum_{i=1}^{\nu} w_i R(u^{(i)}) \tag{23}$$

where R represents the final term of equation (6). The matrices $\tilde{A} = (\tilde{a}_{ij})$, $\tilde{a}_{ij} = 0$ for $j \geq i$ and $A = (a_{ij})$ are $\nu \times \nu$ matrices such that the resulting scheme is implicit in R and is explicit for the spatial derivative operators. In this work, the 4th order version of the above is applied using the implementation in the ARKODE library (Hindmarsh et al., 2005); the appropriate constants, i.e. A, $\tilde{A}$ and ν, may be found in the given the reference.

Results and discussion

Four test problems of increasing difficulty are solved, using the models described in Section 2: firstly, a single component elution with a linear isotherm; secondly, a single component elution with a nonlinear isotherm; thirdly, a two component elution with a nonlinear isotherm and finally a three component displacement chromatographic problem on a large domain. The first of these problems is simulated using the simpler EDM only while, for the second, the EDM and LKM are used in turn; the last two test problems utilise the LKM. In each case, the model is resolved using the numerical method detailed in the previous section. The results obtained both with and without the application

of the PAG method are compared. Additionally, as discussed previously, implicit temporal solvers are typically applied to solve such these problems in the literature. For comparison, solutions are computed both on uniform grids and with PAG using the IDA differential-algebraic equation solver within the Sundials library (Hindmarsh et al., 2005); the uniform grid using the implicit solver is used as a benchmark for the improvements in efficiency made. All simulations are performed using a Intel Xeon CPU E5-2640 v3 (2.60 GHz) 8 Gb memory is used.

Where the PAG method is applied, the finest resolution of the grid is set equivalent to the uniform grid used; furthermore, an initial uniform grid is used for the first 100 time steps after which an adapted grid is constructed after every 100 timesteps; this initial uniform grid is used as, for the majority of the cases investigated, the transients are initiated through their boundary conditions and this initial period allows the dynamic profiles to enter the domain. For all simulations, the time-step of $\Delta t = 5 \times 10^{-4}$ min was used.

Test 1

This test is taken from Javeed et al. (2011b) and is used to analyse the performance of the spatial discretisation presented in the previous section in the context of an convection dominated problem. The test assumes a single-component with a linear isotherm, i.e. $q = ac$. The problem is simulated for 0.6 min and 200 computational cells are used for the uniform grid.

The problem is solved for a column of length 1 cm, that is on the interval $x \in [0, 1]$ cm, with $a = 1$, $v = 1$ cm min^{-1} and $\epsilon = 0.5$, with the following initial conditions assumed:

$$c\left(0, x\right) = \begin{cases} \sin\left(5\pi\left(z - 0.2\right)\right) & \text{if } 0.2 \leq x \leq 0.4, \\ 0 & \text{else} \end{cases} \tag{24}$$

and the left hand boundary condition is set to $c\left(t, 0\right) = 0$. The analytical solution for this problem was presented by Javeed et al. (2011b) as

$$c\left(t, x\right) = -\frac{1}{2}\,\text{real}\left(ie^{p}\left[\text{erf}\left(\alpha\right)\text{erf}\left(\beta\right)\right]\right) \tag{25}$$

where

$$p = 0.5D_a t\left(\frac{\pi}{0.2}\right)^2 + i\frac{\pi}{0.2}\left(0.2 - x - 0.5t\right), \tag{26}$$

$$\alpha = \frac{-0.2 + x - 0.5t}{2\sqrt{0.5D_a t}} - i\pi\frac{\sqrt{0.5D_a t}}{0.2}, \tag{27}$$

$$\beta = \frac{-0.4 + x - 0.5t}{2\sqrt{0.5D_a t}} - i\pi\frac{\sqrt{0.5D_a t}}{0.2}. \tag{28}$$

Figure 1 shows a comparison of the analytical solution with the predictions obtained using the uniform grid and the PAG-linear after 0.6 min; also shown, for reference, is the result obtained using a first order scheme. As can be

observed, both of the simulated results are in excellent agreement, with the PAG-linear and uniform grid predictions superimposed; however in both cases there is an error in the prediction of the peak of the analytical solution. This error is seen to be similar to that shown for the schemes presented in the original reference, and is significantly greater in the results using the first order scheme so is not a result of the adaptive method.

Figure 2 (a) and (b) and present comparisons of predictions obtained with the Implicit and IMEX temporal solvers and with the PAG linear and PAG WENO reconstruction techniques and respectively. As can be seen in Figure 2 (a) difference in the predictions obtained with the two temporal solver is negligible. There is, however, a slight difference in the results from the two reconstructions around the peak of the profile, in order to see this clearly Figure 2 (b) shows only a small interval around this region.

Table 3 presents the CPU runtimes for each of the simulations as well as the runtime reductions relative to the benchmark of a uniform grid with the use of the Implicit solver. As can be seen, the PAG-linear results in a 86.4 % CPU runtime reduction over the benchmark; while, as can be seen in Table 3, PAG-WENO enables a further 10% reduction in the runtime Figure 2 (b) shows there is an additional slight error, resulting in a slight shifting of the peak of the profile. Figure 2 (a) shows that use of the Implicit solver does not result in a change in the predictions, however a significant increase in runtime is observed in Table 3.

Test 2

This case is again taken from Javeed et al. (2011b), and represents the injection of a single component at a rate of $c = 1$ g L^{-1} into a column of length 1 cm, which is initially equilibriated with the solvent $c = 0$, for 0.2 min. The following non-linear isotherm is considered:

$$q(c) = \frac{c}{1+c}. \tag{29}$$

The values for v and ϵ are the same as those for Test 1 and the same number of computational cells is used, while in this case the solution is computed for 3 min. In order to assess the ability of the compact WENO scheme coupled with PAG method to simulate problems where both the EDM and LKM are used, this problem will be solved using both of these models in turn. Where the LKM is applied k is assumed to take the value 10^3. The CPU runtimes for simulations using both models are summarised in Table 4.

EDM

Figure 3 shows a comparison of the predicted concentration close to the end of the bed ($x = 0.95$) obtained using uniform, PAG-linear, and PAG-WENO grids. Also shown, in the absence of an analytical solution to the problem, is a reference solution which obtained using a uniform grid of 2000 computational cells. From the figure it can clearly be observed that use of a relatively small mesh size results in an under-prediction of the concentration peak, nevertheless the use of the PAG method does not accentuate this problem and, as shown in Table 4, results in a 20 - 30 % reduction in runtime though, as seen in Test 1, the use of the PAG-WENO results in a delay in the time at which the profile reaches the point at which the histories are presented. Furthermore, as with Test 1, the two temporal solvers produced

identical results.

LKM

As in the case of the EDM above, Figure 4 (a) shows the comparisons of the predicted concentration histories at $x = 0.95$ using the uniform grid as well as PAG-linear and PAG-WENO reconstructions while Figure 4 (b) presents the same comparison for the IMEX and implicit solvers.

Notably, the maximum of the peak is lower with the use of the LKM than is seen with the EDM, which is due to the delay in adsorption incorporated into the model; also the predictions with smaller grids are in much better agreement with the reference solution.

As with the above cases, 4 (a) shows that the WENO reconstruction results in a slight delay in the propagation of the front; furthermore, the implicit solver also slightly increases the diffusion of the peak of the profile. As can be seen in Table 4 the runtimes associated with all of the LKM simulations are significantly lower than those for the EDM, which is as a result of the removal of the nested solution of the algebraic equation (5), with the PAG-linear method resulting in a further 30 % decrease.

Test 3

As both Tests 1 and 2 were concerned with single components for Test 3 we select the problem presented by Shipilova et al. (2008) where the LKM is applied to a two component system. In this case a competitive Langmuir isotherm is used, that is for component n:

$$q_n(\mathbf{c}) = \frac{a_n c_n}{1 + \sum_j b_j c_j} \tag{30}$$

A rectangular pulse of a liquid mixture containing the two components is injected into the column for the first 1.2 min of the problem; after this period the concentration of the two components in the incoming stream drops to zero. Table 1 presents the various parameters used, as with the previous tests, 200 computational cells were used for the uniform grid and 4 min of the problem were simulated. Table 5 shows the CPU runtimes recorded in each case.

Figures 5 (a) and (b) show respectively a comparison of the predictions produced using a uniform grid and the PAG-linear and PAG-WENO, and the comparison of the results obtained by applying the IMEX and Implicit solvers respectively. As can be seen in 5 (a), as in the above cases, the predictions obtained using the PAG method are in reasonable agreement with those from the uniform grid. There are two exceptions worth noting: firstly, where PAG-linear is used, the end of the rectangular pulse at approximately 2 min is diffused, with the drop in concentration beginning 0.4 min before that in observed in the uniform solution, the same effect using the WENO reconstruction is almost negligible; secondly, that the PAG-WENO shows a slight delay in the arrival of the sharp front at *ca.* 0.7 min. Likewise, Figure 5 (b) shows that implicit PAG-linear solution provides a far better resolution of the solution around 2 min, but diffuses the front at 0.7 min to a greater extent.

Figure 6 shows the same results of the PAG-linear and PAG-WENO obtained using the IMEX solver, this time obtained using an initial grid of 1000 cells. As can be seen, even with the greater number of cells the PAG-linear

diffuses the wave at 2 min, while in contrast the PAG-WENO accurately resolves all parts of the solution. In this case the simulation was only performed using the IMEX solver.

From Table 5, firstly, it can been seen that the implicit solver required runtimes at least 10 times longer than the equivalent for the IMEX solver. For the finer grid simulations, where comparison is given against a uniform grid with the IMEX solver only, less of a runtime reduction was observed as compared to the coarser grid.

Test 4

The previous tests have investigated problems on a small interval, for Test 4 we analyse the three component displacement problem presented by Javeed et al. (2011a) which uses a much larger column length. This problem consists of the injection of a rectangular pulse of the first two components (c_1 and c_2) for 0.2 s, without the presence of the third component, followed by the injection of only the third displacer component. The key parameters and feed compositions are presented in Table 2. In this test, due to the larger domain, 1000 computational cells were used for the uniform grid while the simulation time was 18 min.

Figure 7 presents profiles of the the solution obtained using a uniform grid with the IMEX solver at $t = 1$, 4, 8, 12 and 16 min. As can be seen the pulses, of components 1 and 2 propagate through the domain and are resolved into rectangular pulses of pure components by the second half of the domain. Figures 8 (a) and (b) show comparisons of the uniform grid predictions with the PAG-linear grid at the same times for the components 1 and 2 respectively, as with the previous tests the error associated with the adaptive grid is negligible but results in a 66 % reduction in runtime (Table 6). Also shown are the PAG-linear predictions obtained using the Implicit solver, the results are similar although, as can be seen in Figure 8c as before the implicit solver results in an increased diffusion around the discontinuities; as before the runtime required for the implicit is over twice that for the IMEX.

Conclusions

The simulation of chromatographic separation problems requires the solution of a system of nonlinear partial differential-algebraic equations. Regardless of the model applied, a particular complexity of the equations is that, under certain conditions, discontinuous profiles or shocks can form; the resolution of such profiles is challenging and requires the selection of an appropriate accurate numerical scheme, while being careful to maintain computational efficiency.

This paper presented the application of a high order numerical method which is coupled with the Piecewise Adaptive Grid method (PAG) in order to reduce the additional computational overhead associated with its use. Importantly, due to the nonuniform structure of grid used as part of the PAG method, the particular numerical scheme selected, a compact WENO method, was one of the few applicable to such grids. To further increase the efficiency while improving the accuracy of predictions, the impact of the use of explicit and Implicit-Explicit (IMEX) Runge-Kutta as compared to the commonly applied fully implicit BDF method was investigated.

Application of the scheme to the simpler Equilibrium Dispersive Model (EDM) for single component, smooth and discontinuous problems showed that an efficiency penalty, in terms of the CPU runtime, is observed relative to the

simpler first order methods; however the accuracy of solutions, for relative coarse meshes is far greater, as is expected. The PAG method goes some way to mitigate the increase in decrease in efficiency even for the simplest problems, by reducing the runtime by up to *ca.* 35 %, without an observable deterioration in the solution. It was found that the explicit temporal solver was up to 6 times more efficient that the implicit solver.

Extension to problems where the Lumped Kinetic Model was applied, and hence the use of an IMEX rather than a explicit Runge-Kutta method, showed an increase in efficiency over the EDM. As the problems with a greater number of components were investigated a larger reduction in the CPU runtime was observed with the application of the PAG method; this is due to the greater computational weight per cell in the grid used, in a similar manner to the results observed in Brown et al. (2015b).

Finally, the reconstruction of the solution required following the construction of the new grid, part of the PAG algorithm (Brown et al., 2015b), using the underlying WENO reconstruction rather than the linear interpolation used in our previous work resulted in an increase in computational efficiency. Overall, the use of PAG for industrially relevant problems requiring an implicit solver resulted in upto 90% fall in runtime.

References

Ascher, U., Ruuth, S., Spiteri, R., 1997. Implicit-explicit Runge-Kutta methods for time-dependent partial differential equations. Applied Numerical Mathematics 25 (2-3).

Berger, M., Oliger, J., 1984. Adaptive mesh refinement for hyperbolic partial differential equations. J. Comput. Phys. 53 (3), 484–512.

Brown, S., Fraga, E., Mahgerefteh, H., Martynov, S., 2015a. A geometrically based grid refinement technique for multiphase flows. Computers & Chemical Engineering 82, 25–33.

Brown, S., Martynov, S., Mahgerefteh, H., 2015b. Modelling heat transfer in flashing CO_2 fluid upon rapid decompression in pipelines. In: Proceedings of 8th International Conference on Computational and Experimental Methods in Multiphase and Complex Flow. To appear.

Brown, S., Martynov, S., Mahgerefteh, H., Chen, S., Zhang, Y., 2014. Modelling the non-equilibrium two-phase flow during depressurisation of CO_2 pipelines. Int. J. Greenhouse Gas Control 30, 9–18.

Butcher, J., 2008. Numerical Methods for Ordinary Differential Equations. Wiley.

Chan, S., Titchener-hooker, N., Bracewell, D. G., Sørensen, E., 2008. A Systematic Approach for Modeling Chromatographic Processes âĂŤ Application to Protein Purification 54 (4), 965–977.

Close, E. J., Salm, J. R., Bracewell, D. G., Sorensen, E., jul 2014. Modelling of industrial biopharmaceutical multicomponent chromatography. Chemical Engineering Research and Design 92 (7), 1304–1314.
URL http://www.sciencedirect.com/science/article/pii/S0263876213004425

Coimbra, M. d. C., Sereno, C., Rodrigues, A., 2004. Moving finite element method: applications to science and engineering problems. Computers & Chemical Engineering 28 (5), 597–603.
URL http://linkinghub.elsevier.com/retrieve/pii/S0098135404000286

Enmark, M., Arnell, R., Forssén, P., Samuelsson, J., Kaczmarski, K., Fornstedt, T., 2011. A systematic investigation of algorithm impact in preparative chromatography with experimental verifications. Journal of Chromatography A 1218 (5), 662–672.
URL http://dx.doi.org/10.1016/j.chroma.2010.11.029http://linkinghub.elsevier.com/retrieve/pii/S0021967310016031

Fraga, E. S., 1998. Simulation of a fixed bed system using a geometrically based adaptive grid method. Comput. Chem. Eng. 22, 897–900.

Fraga, E. S., Morris, J. L., Jul. 1992. An adaptive mesh refinement method for nonlinear dispersive wave equations. J. Comput. Phys. 101 (1), 94–103.

Fraga, E. S., Morris, J. L., 1996. A piecewise uniform adaptive grid algorithm for nonlinear dispersive wave equations. In: Griffiths, D. F., Watson, G. A. (Eds.), Numerical Analysis: A R Mitchell 75*th* Birthday Volume. World Scientific Publishing Company, Singapore, pp. 99–124.

Gourma, M., Jia, N., Thompson, C., 2013. Adaptive mesh refinement for two-phase slug flows with an *a priori* indicator. Int. J. Multiphase Flow 49, 83–98.

Guiochon, G., Shirazi, D., Felinger, A., Katti, A., 2006. Fundamentals of Preparative and Nonlinear Chromatography. Academic Press.

Hahn, T., Sommer, A., Osberghaus, A., Heuveline, V., Hubbuch, J., 2014. Adjoint-based estimation and optimization for column liquid chromatography models. Computers & Chemical Engineering 64, 41–54.

Hindmarsh, A. C., Brown, P. N., Grant, K. E., Lee, S. L., Serban, R., Shumaker, D. E., Woodward, C. S., 2005. Sundials: Suite of nonlinear and differential/algebraic equation solvers. ACM Transactions on Mathematical Software (TOMS) 31 (3), 363–396.

Javeed, S., Qamar, S., Seidel-Morgenstern, A., Warnecke, G., 2011a. A discontinuous Galerkin method to solve chromatographic models. Journal of Chromatography A 1218 (40), 7137–7146.

Javeed, S., Qamar, S., Seidel-Morgenstern, A., Warnecke, G., 2011b. Efficient and accurate numerical simulation of nonlinear chromatographic processes. Computers & Chemical Engineering 35 (11), 2294–2305.

Kelling, R., Bickel, J., Nieken, U., Zegeling, P., 2014. An adaptive moving grid method for solving convection dominated transport equations in chemical engineering. Comput. Chem. Eng. 71, 467–477.

Levy, D., Puppo, G., Russo, G., 2000. Compact central weno schemes for multidimensional conservation laws. SIAM J. Sci. Comput. 22 (2), 656–672.

Mazzotti, M., 2009. Nonclassical composition fronts in nonlinear chromatography: Delta-shock. Industrial and Engineering Chemistry Research 48 (16), 7733–7752.

Medi, B., Amanullah, M., 2011. Application of a finite-volume method in the simulation of chromatographic systems: Effects of flux limiters. Industrial and Engineering Chemistry Research 50 (3), 1739–1748.

Pais, L. S., Loureiro, J. M., Rodrigues, a. E., 1998. Modeling strategies for enantiomers separation by SMB chromatography. AIChE Journal 44 (3), 561–569.

Pelanti, M., LeVeque, R. J., Jan. 2006. High-Resolution Finite Volume Methods for Dusty Gas Jets and Plumes. SIAM J. Sci. Comput. 28 (4), 1335–1360.

Püttmann, A., Schnittert, S., Leweke, S., von Lieres, E., 2016. Utilizing algorithmic differentiation to efficiently compute chromatograms and parameter sensitivities. Chemical Engineering Science 139, 152–162.

Russell, R. D., Christiansen, J., 1978. Adaptive mesh selection strategies for solving boundary value problems. SIAM Journal on Numerical Analysis 15 (1), 59–80.

Semplice, M., Coco, A., Russo, G., 2015. Adaptive Mesh Refinement for Hyperbolic Systems Based on Third-Order Compact WENO Reconstruction. Journal of Scientific Computing.

Sereno, C., Rodrigues, A., Villadsen, J., 1991. The moving finite element method with polynomial approximation of any degree. Computers and Chemical Engineering 15 (1), 25–33.

Shipilova, O., Sainio, T., Haario, H., 2008. Particle transport method for simulation of multicomponent chromatography problems. Journal of Chromatography A 1204 (1), 62–71.

Tang, H., Tang, T., 2003. Adaptive Mesh Methods for One- and Two-Dimensional Hyperbolic Conservation Laws. SIAM Journal on Numerical Analysis 41 (2), 487.

von Lieres, E., Andersson, J., 2010. A fast and accurate solver for the general rate model of column liquid chromatography. Computers & Chemical Engineering 34 (8), 1180–1191.

Zabusky, N., Kruskal, M., Aug 1965. Interaction of "solitons" in a collisionless plasma and the recurrence of initial states. Phys. Rev. Lett. 15, 240–243.

Zhang, Y., Feng, L., Seidel-Morgenstern, A., Benner, P., 2017. Accelerating optimization and uncertainty quantification of nonlinear SMB chromatography using reduced-order models. Computers and Chemical Engineering 96, 237–247.

URL http://dx.doi.org/10.1016/j.compchemeng.2016.09.017

Table 1: Parameters used in Test 3.

Parameters	Value
Column length (cm)	1
Porosity	0.4
Velocity (cm min^{-1})	1
Dispersion Coefficient (cm^2 min^{-1})	10^{-4}
Lumped mass transfer coefficient (min^{-1})	10^3
Henry coefficients	$a_1 = 0.5$, $a_2 = 1$
Constants used in Eq (3)	$b_1 = 0.05$, $b_2 = 0.1$
Feed concentrations (gl^{-1})	$c_1 = 10$, $c_2 = 10$

Table 2: Parameters used in Test 4.

Parameters	Value
Column length (cm)	100
Porosity	0.5
Dispersion Coefficient (cm^2 min^{-1})	10^{-4}
Adsorption rate (min^{-1})	10^3
Henry coefficients	$a_1 = 4$, $a_2 = 5$, $a_3 = 6$
Constants used in Eq (3)	$b_1 = 4$, $b_2 = 5$, $b_3 = 1$
Feed concentrations (gl^{-1}) ($t < 0.1$)	$c_1 = 1$, $c_2 = 1$, $c_3 = 0$
Feed concentrations (gl^{-1}) ($t \geq 0.1$)	$c_1 = 0$, $c_2 = 0$, $c_3 = 1$

Table 3: Summary of CPU runtimes in seconds and % reduction in runtimes relative to the Implicit uniform grid solution for Test 1.

Temporal Solver	Implicit		IMEX	
	CPU runtime	% reduction	CPU runtime	% reduction
Uniform Grid	291.6	-	53.0	81.8
PAG-linear	256.3	12.1	39.6	86.4
PAG-WENO	276.8	5.1	34.0	88.3

Table 4: Summary of CPU runtimes in seconds and % reduction in runtimes relative to the Implicit uniform grid solution for Test 2.

Temporal Solver	Implicit		IMEX	
	CPU runtime	% reduction	CPU runtime	% reduction
		EDM		
Uniform Grid	941.9	-	167.7	82.2
PAG-linear	892.4	5.3	133.8	85.8
PAG-WENO	884.7	6.1	120.5	87.2
		LKM		
Uniform Grid	289.2	-	12.1	95.8
PAG-linear	243.6	15.8	8.4	97.1
PAG-WENO	-	-	11.9	95.9

Table 5: Summary of CPU runtimes in seconds and % reduction in runtimes relative to the Implicit and IMEX uniform grid solutions for 200 and 1000 cells respectively for Test 3.

Temporal Solver	Implicit		IMEX	
	CPU runtime	% reduction	CPU runtime	% reduction
		200 cells		
Uniform Grid	941.9	-	97.5	89.6
PAG-linear	884.7	6.1	58.3	93.8
PAG-WENO	-	-	50.4	94.6
		1000 cells		
Uniform Grid	-	-	320.2	-
PAG-linear	-	-	242.9	24.1
PAG-WENO	-	-	242.1	24.4

Table 6: Summary of CPU runtimes in seconds and % reduction in runtimes relative to the Implicit uniform grid solution for Test 4

Temporal Solver	Implicit		IMEX	
	CPU runtime	% reduction	CPU runtime	% reduction
Uniform Grid	424.5	-	165.4	61.0
PAG-linear	205.6	51.6	70.5	83.4

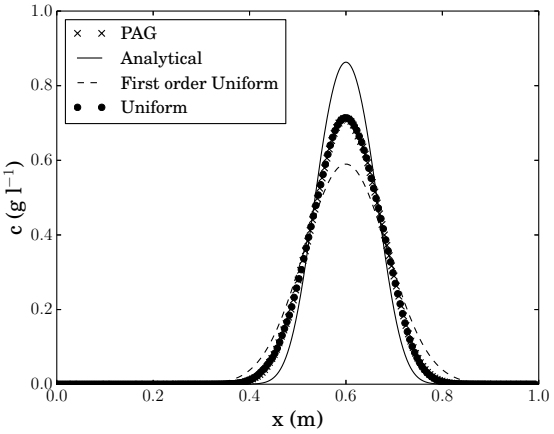

Figure 1: Comparison of the analytical solution with the numerical solutions for c for Test 1 computed using a uniform grid of 200 cells and an equivalent piecewise adaptive grid with a linear reconstruction (PAG-linear) at $t = 0.6$ min.

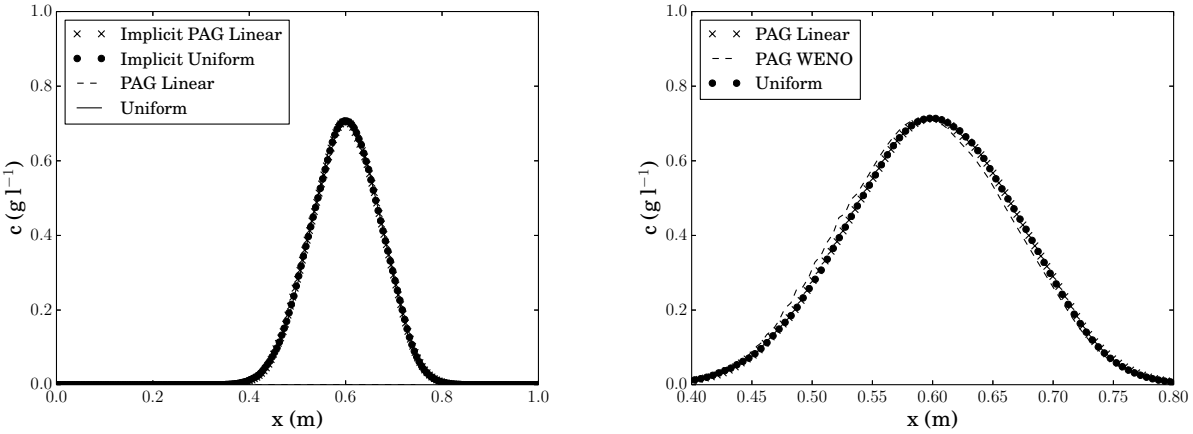

(a) (b)

Figure 2: Comparison of the numerical solutions for c computed for Test 1 using (b) PAG with linear and WENO interpolations applied for the reconstruction (a) Implicit-explicit (IMEX) and implicit temporal solvers respectively.

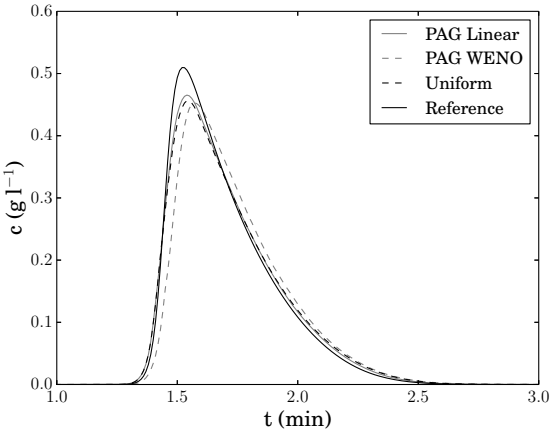

Figure 3: Predicted variation of c with time at $x = 0.95$ cm computed using the Equilibrium Dispersive Model (EDM) for Test 2 with a uniform grid, as well as PAG-linear and PAG-WENO reconstructions also shown is a reference solution obtained using 2000 uniform cells.

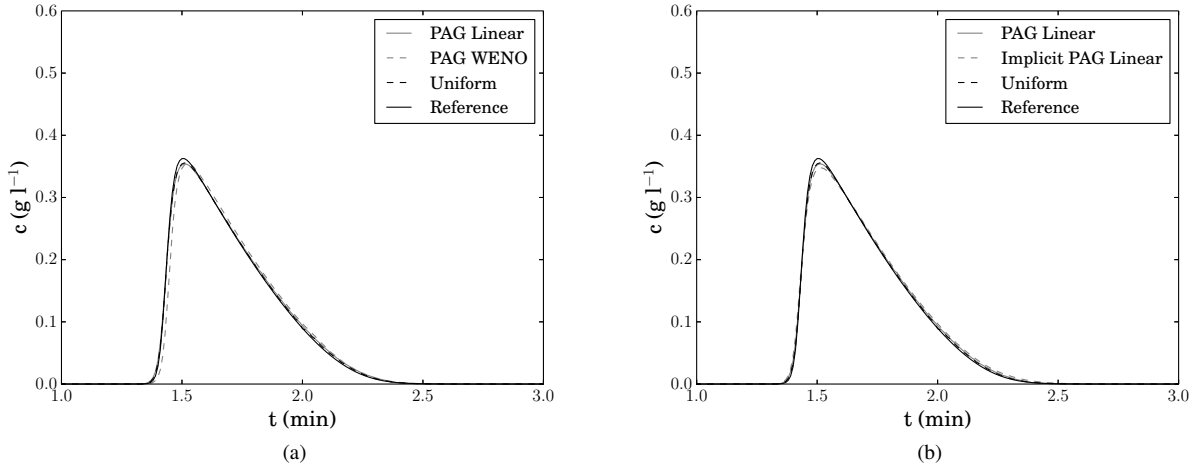

Figure 4: Predicted variation of c with time at $x = 0.95$ cm computed using the LKM with $k = 10^3$ for Test 2 using (a) a uniform grid, as well as PAG-linear and PAG-WENO reconstructions (b) IMEX and implicit solvers respectively; also shown is a reference solution obtained using 2000 uniform cells.

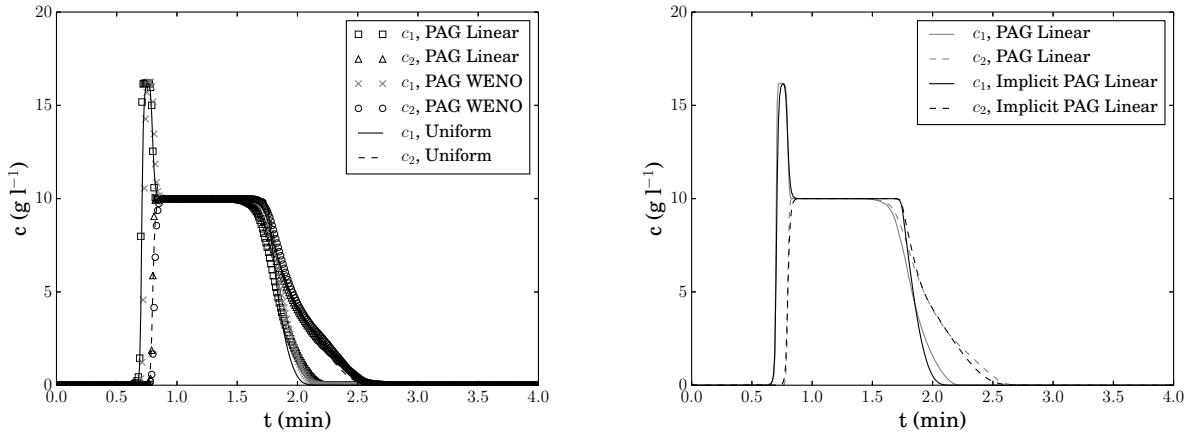

(a) (b)

Figure 5: Predicted variation of c_1 and c_2 with time at $x = 0.5$ cm for Test 3 with (a) a uniform grid, as well as PAG-linear and PAG-WENO reconstructions (b) IMEX and implicit solvers respectively; also shown is a reference solution obtained using 2000 uniform cells.

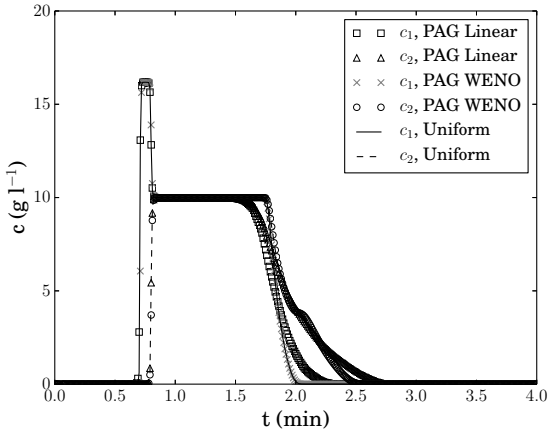

(a)

Figure 6: Predicted variation of c_1 and c_2 with time for Test 3 at $x = 0.5$ cm using a uniform grid, as well as PAG-linear and PAG-WENO reconstructions with an equivalent uniform grid of 1000 computational cells.

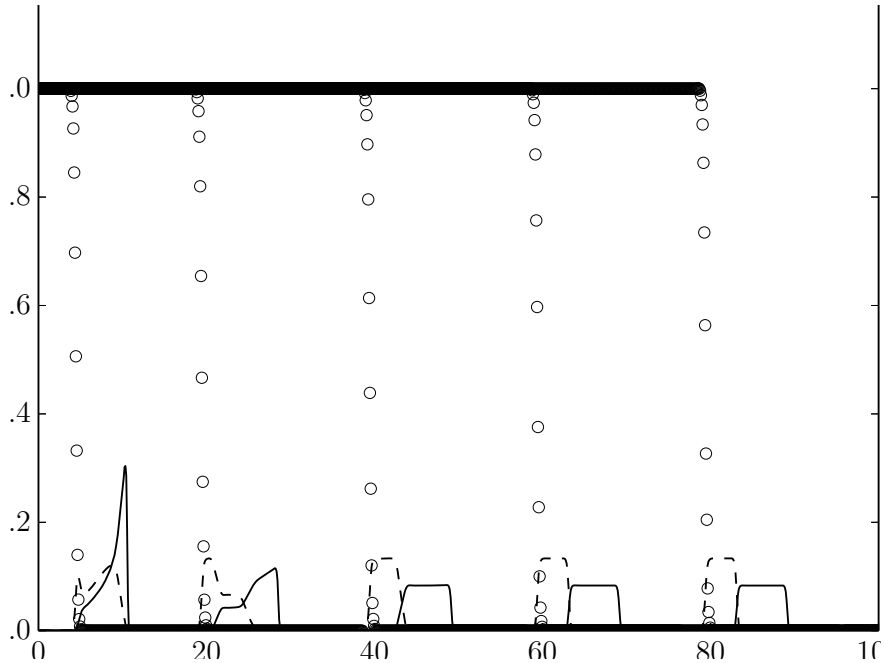

Figure 7: Variation of c_1, c_2 and c_3 along the length of the bed at 1, 4, 8, 12 and 16 min for Test 4 predicted using a uniform grid of 1000 computational cells.

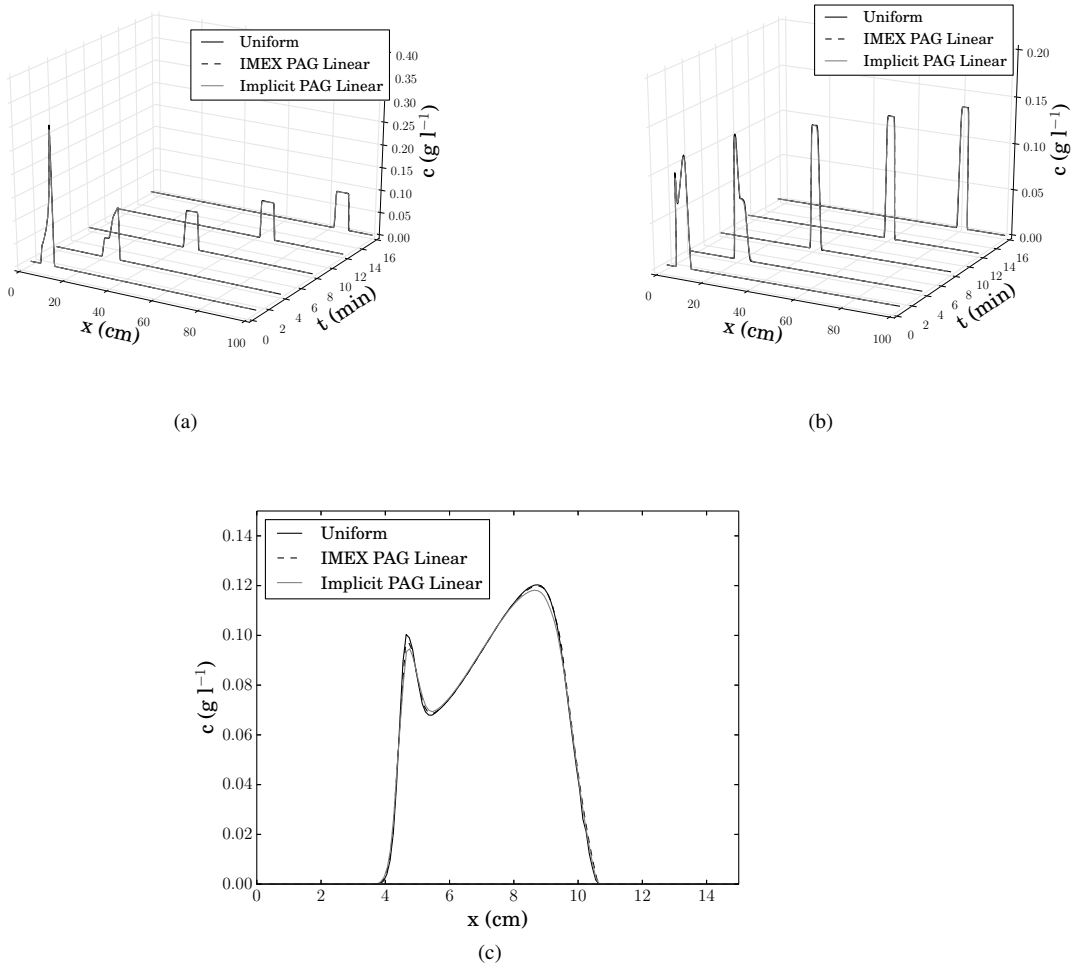

Figure 8: Variation of c_1 (a) and c_2 (b) along the length of the bed at 1, 4, 8, 12 and 16 min predicted using the IMEX and implicit temporal solvers using the PAG-linear method, (c) shows the profile of c_2 between 0 and 15 cm at 1 min.